IEEE Photonics Journal
An IEEE Photonics Society Publication

Open Access

Vertically Coupled Partially Tapered Ridge Waveguide Semiconductor FP Laser With Improved Divergence Angles

Volume 12, Number 5, October 2020

Mingwen Lan
Xun Li, ***Senior Member, IEEE***

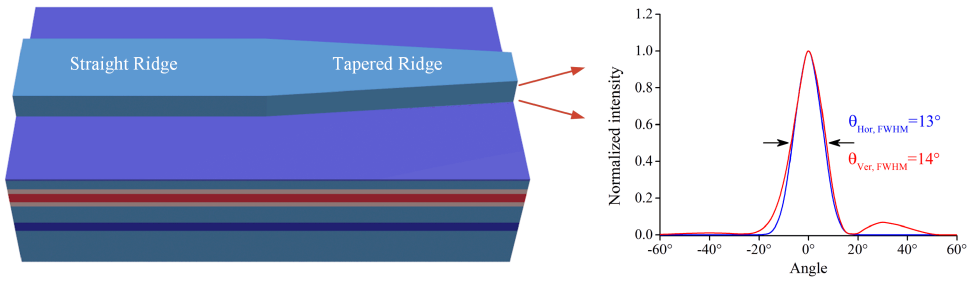

DOI: 10.1109/JPHOT.2020.3028867

IEEE photonics SOCIETY
IEEE

Vertically Coupled Partially Tapered Ridge Waveguide Semiconductor FP Laser With Improved Divergence Angles

Mingwen Lan[1] **and Xun Li**[2,3] ***Senior Member, IEEE***

[1]Wuhan National Laboratory for Optoelectronics, Huazhong University of Science and Technology, Wuhan 430074, China
[2]Department of Electrical and Computer Engineering, McMaster University, Hamilton, ON L8S 4K2, Canada
[3]School of Information Science and Engineering, Shandong University, Qingdao 266237, China

DOI:10.1109/JPHOT.2020.3028867

Manuscript received June 19, 2020; revised September 24, 2020; accepted October 1, 2020. Date of publication October 5, 2020; date of current version October 16, 2020. Corresponding author: Xun Li (e-mail: lixun@mcmaster.ca).

Abstract: In this work, we present a semiconductor FP laser design with significantly reduced divergence angles particularly in the vertical direction. The laser has a pair of vertically stacked, propagation constant unmatched twin waveguides that is coupled by a tapered ridge at the output end. As such, the laser has a significantly extended mode profile at the output section while the light propagation in the main section is not affected. Our simulation result shows that the divergence angles can be reduced to 13° × 14° (horizontal × vertical), as opposed to typical values of 20° × 29° in conventional ridge waveguide laser structures without a sport size convertor integrated. This design does not need any regrowth, with no appreciable penalty brought to other laser characteristics either.

Index Terms: Coupled mode theory, semiconductor lasers, divergence angles.

1. Introduction

Facing massive data transmission demand, ridge waveguide (RW) semiconductor Fabry-Perot (FP) laser with outstanding performance is indispensable. The merits, such as simple structure, high yield, and low fabrication and operation costs, are key factors for their unfailing lives in fiber-optic data links and/or optical interconnects. However, its large divergence angles and high aspect ratio (non-circular shape) leads to a low coupling efficiency to fiber.

Conventional approaches to solve this problem are to co-package micro-lens [1]–[3], or to exploit the fiber tip-lens [4], or to monolithically integrate a spot-size convertor (SSC) [5], or to modify the waveguide by incorporating designs such as the diluted waveguide [6]–[10], or the anti-resonant reflecting optical waveguide (ARROW) [11], or the slab-coupled waveguide (SCW) [12], or photonic bandgap crystal (PBC) waveguide [13], [14]. These methods, however, suffer from either high fabrication costs or low fabrication yield. The modification on waveguide usually jeopardize the laser performance. For example, the SSC integrated in the device front end will need complicated manufacturing processes, which not only brings in the low yield and high cost, but also increases the risk of device degradation. In fabrication of PBC waveguides, the accumulated dislocations in the thick waveguide layer roll down the material integrity significantly, especially in the design of a

waveguide with periodical layers [14]. In the SCW structure, the required etching-through process generates defects in the close vicinity of the active region, which deteriorates the device long-term reliability [15]. As for the lasers with modified waveguide structures, the dramatically increased threshold current is a common disadvantage due to the greatly reduced confinement factor.

Aiming at reducing the coupling loss without sacrificing the device performance, an invention [16] successfully reduced the divergence angles by taking advantage of a staircase naturally formed by its etched-facet technology. Nevertheless, the staircase and the position of the fiber need to be precisely adjusted to avoid multiple peaks in its far-field pattern caused by misalignment of the reflected side lobes, which brings back the low fabrication yield issue.

There are still sophisticated designs such as the buried heterostructure (BH) [17], [18], in which the active region stripe was tapered with its width greatly reduced. As such, its mode profile is almost rounded, and so the far-field pattern is. Its far-field divergence angles are also greatly reduced. Due to these features, the BH structure gain advantages in fiber-coupling over the RW structure, in which the far-field pattern is elliptical with significantly larger divergence angles. However, restricted by the optimum design on other device aspects, such as the optical confinement factor and carrier injection, the vertical divergence angle can hardly be further reduced due to lacking degrees of freedom. However, the fabrication of BH structure requires sophisticated regrowth technology especially in burying of the tapered active region stripe with Al-contained layers, which makes it less cost-effective as compared to the RW structure. Straight stripe BH structure (without tapering) makes the regrowth easier, but it also loses its ability in reducing the far-field divergence angles. To achieve a best fiber-coupling result, a ball lens or integration to an SSC is usually required [19], which will, however, increase the cost again.

In this letter, we present an unmatched vertically stacked twin-waveguide structure by inserting yet another slab waveguide underneath the active region in the conventional RW FP laser. By altering the ridge width along the cavity, we manage to make a coupling of the traveling light wave between the two waveguides nearby the front facet only. As such, the inserted extra waveguide does not take any effect to the main resonance hence the original laser performance will be preserved. As it approaches to the front facet, the light wave will be partially coupled to the extra waveguide, which expands the mode spot size and consequently reduces the divergence angles. The proposed design only needs a single step epitaxial growth plus normal wafer processing technology. It is fully compatible with the manufacturing technology of conventional RW semiconductor FP lasers.

The rest of this paper is organized as follows. The device structure and its working principle is introduced in Section 2. Section 3 describes the design optimization of the entire waveguide. Simulated device performance is shown in Section 4. Finally, a conclusion of this work is summarized in Section 5.

2. Device Structure and Working Principle

Inspired by the coupled mode theory, which has been applied in many coupled waveguide designs, such as the adiabatic mode transformer [20], [21] and the silicon/III-V hybrid devices [22], [23], we propose our structure as shown in Fig. 1(a). In the vertical (epitaxial) direction, the proposed laser consists of two propagation constant unmatched waveguides: a conventional ridge waveguide and an underneath slab waveguide with a low refractive index space layer in between. Along the cavity (in the light propagation direction), the laser has two sections: a straight ridge section (SRS) and a tapered ridge section (TRS). The SRS is the same as the conventional RW laser with a uniform ridge, whereas the TRS has a horn-like gradually narrowed ridge along the cavity as shown in Fig. 1(b). The cross-sectional views of the ridge in different sections are exhibited in Figs. 1(c) and (d), respectively.

Since the two waveguides are unmatched in the SRS, the fundamental mode excited in the top ridge waveguide will not be coupled to the underneath slab waveguide. Hence the latter has little effect on the mode confinement and the SRS shows no difference from a conventional RW laser. Consequently, the laser performance will not be affected in the SRS. In the TRS, however,

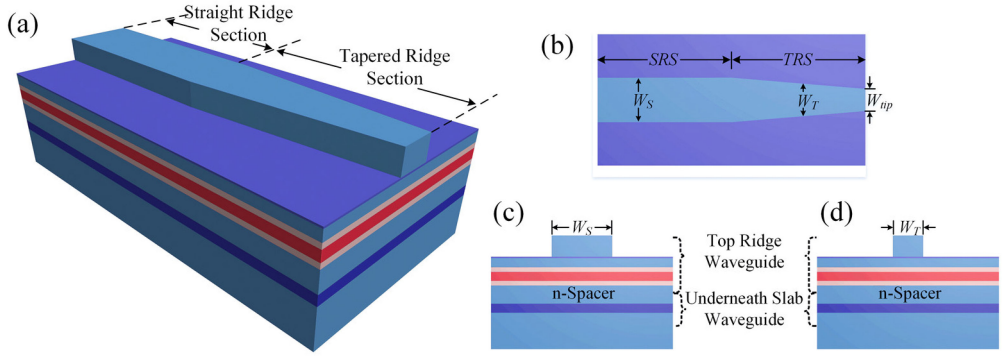

Fig. 1. (a) The schematic illustration of the proposed structure. (b) The top view of the structure, (c) and (d) the cross-sectional views of the SRS and TRS, respectively.

as the ridge width reduces, the propagation constant of the top ridge waveguide is approaching to that of the slab waveguide. The fundamental mode is therefore gradually coupled from the top ridge waveguide to the underneath slab waveguide. Once the coupling sends about half of the light power to the slab waveguide, we cut off the waveguide and set this position as the front (output) facet. As such, the mode distribution area reaches its maximum at the output facet and is largely expanded in all directions in the cross-sectional area. We can then obtain a pair of significantly reduced far-field divergence angles in both horizontal and vertical directions, specifically in the vertical direction. It's worth mentioning that, unlike other tapered twin waveguide structures that enforce a complete transfer of the light power from the top to the underneath waveguide, such as the TRAFFiC structure [24], the ATG structure [25], and the hybrid III-V on silicon laser [26], [27], the proposed structure will take a much shorter taper length, as only about a half power transfer is required. For the same reason, we managed to achieve a design without extension of the total laser cavity length (200 μm), which makes it possible to improve the divergence angles of the FP laser without serious deteriorating its other performance.

3. Structure Design and Optimization

Since the fabrication of conventional RW FP lasers has been a mature technology, we will avoid any change on the design of the top ridge waveguide that comprises the strained-layer multiple quantum well (SL-MQW) active region, the top and bottom graded-index separate confinement hetero-structure (GRINSCH), and the top and bottom InAlAs blocking layers. We only need to design the underneath slab waveguide in conjunction with the ridge in the TRS. A typical set of design parameters for the cross-sectional structure are listed in Table 1, with the thicknesses of the underneath slab waveguide core layer and the N-spacer to be determined by the followed optimization process.

3.1 Design Optimization of the Slab Waveguide Core Layer

We have followed two principles in choosing the thickness of the core layer in underneath waveguide: (a) in the SRS, the core layer has as little effect to the top ridge waveguide as possible; (b) in the TRS, the two waveguides can have their propagation constants (i.e., effective indices) gradually matched.

Fig. 2(a) shows the calculated effective index of the individual top ridge waveguide (with the underneath slab waveguide removed) as a function of its ridge width, and the individual underneath slab waveguide (with the top ridge waveguide removed) as a function of the core layer thickness. The material of the slab waveguide core layer is chosen to be the same as that of the etching stop

TABLE 1
Cross-Sectional Structure Parameters

Name	Material	Thickness (nm)	Refractive index (at 1.31μm)
Cap	InGaAs	200	3.61
P-cladding	InP	1800	3.21
Etching stop layer	InGaAsP	10	3.34
P-spacer	InP	80	3.21
P-blocking layer	InAlAs	40	3.20
Top GRINSCH	InAlGaAs	60	3.26
Barriers	InAlGaAs	8.5×10	3.36
Wells	InAlGaAs	5×9	3.38
Bottom GRINSCH	InAlGaAs	60	3.26
N-blocking layer	InAlAs	40	3.20
N-spacer	InP	d_1	3.21
Slab waveguide core layer	InGaAsP	d_2	3.34
Buffer	InP	500	3.21
Substrate	InP	-	3.21

$*d_1$, d_2: parameters to be determined

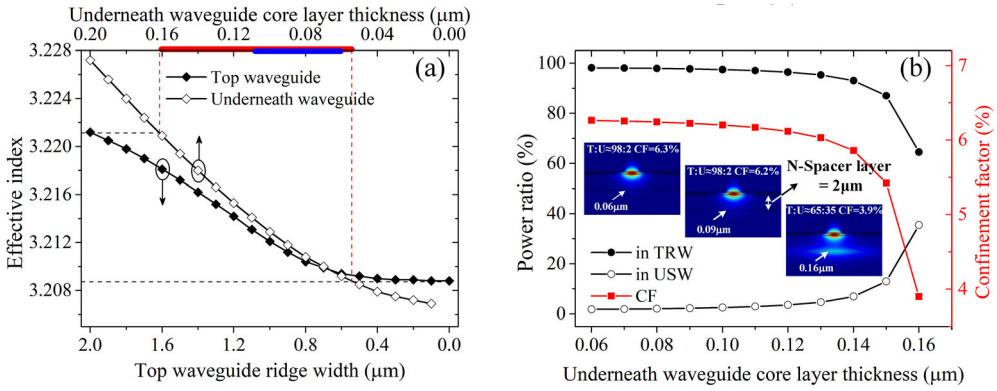

Fig. 2. (a) Effective index of the top waveguide versus its ridge width, and that of the underneath slab waveguide versus its core layer thickness. (b) Power ratio of the fundamental mode in the top ridge and underneath slab waveguide, and the confinement factor (CF) as functions of the underneath waveguide core layer thickness in the SRS. (Insets: the mode patterns under three different core layer thicknesses, TRW: top ridge waveguide, USW: underneath slab waveguide).

layer, to make it have a higher material refractive index than the InP N-spacer but transparent at the operating wavelength of 1.31 μm.

In Fig. 2(a), it is apparent that the thickness of the underneath waveguide core layer can take any value from 0.06 μm to 0.16 μm, in order to match the effective index as required by above principle (b), as shown by the red bar marked along the top horizontal axis in Fig. 2(a). However, as the core layer is getting thicker, the effective index matching will happen when the top waveguide ridge width is approaching to 2 μm, the value of the SRS. As such, above principle (a) could be jeopardized since the guided wave by the top ridge waveguide could be coupled to the underneath slab waveguide in the SRS. This unwanted coupling would reduce the confinement factor and consequently result a higher threshold current as well as a lower slope efficiency of the FP laser.

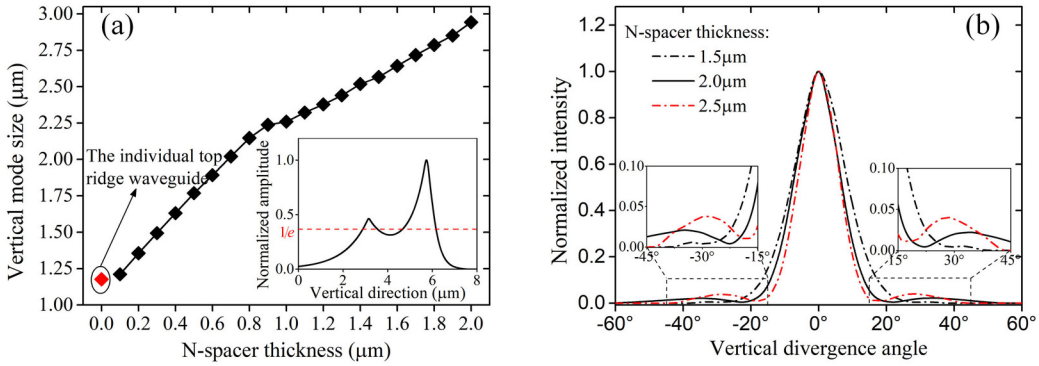

Fig. 3. (a) Vertical mode size dependence on the N-spacer thickness. (b) Far-field patterns along the vertical direction with different N-spacer thicknesses.

To find the optimized value, we then calculated the effect of the core layer thickness on the mode distribution in the SRS. The result is shown in Fig. 2(b).

It is found that as the core layer thickness of the underneath waveguide increases, the field guided by the top ridge structure will be pulled down in the SRS, which decreases the confinement factor of the top ridge structure and deteriorates the laser performance as mentioned above. Nevertheless, once the core layer thickness is less than 0.11 μm, the mode distribution no longer changes appreciably as demonstrated in Fig. 2(b). For an eclectic choice, we select 0.09 μm as the thickness of the core layer, which roughly stays in the middle of the matching range left over, shown as the blue bar in Fig. 2(a).

3.2 Design Optimization of the N-Spacer

In a vertically coupled twin-waveguide structure, the distance between the two waveguides is crucial to mode coupling. It is also apparent that the mode expands with the thickness of the N-spacer. Hence a thicker N-spacer will lead to an extended mode size and consequently small far-field divergence angles. Fig. 3(a) shows the calculated dependence of the fundamental mode size along the vertical direction on the N-spacer thickness, where the slab waveguide core layer thickness and the top ridge waveguide width have been chosen as 0.09 μm and 0.97 μm, respectively, with their propagation constants matched to each other. As expected, the fundamental mode size along the vertical direction indeed expands with the N-spacer. However, the N-spacer cannot be overly thick, as otherwise a dimple appears between the twin peaks confined by the top ridge waveguide and the slab waveguide, respectively. As the thickness of the N-spacer exceeds 2.0 μm, the dimple drops to over *1/e* of the peak value as shown in the inset of Fig. 3(a), leading to little improvement on the divergence angle but noticeable side lobes as shown in Fig. 3(b), which jeopardizes the far-field pattern along the vertical direction. We therefore set the N-spacer thickness to 2.0 μm for a best trade-off between the divergence angle and the quality of the far-field pattern.

3.3 Design Optimization of the TRS Length

To obtain the optimized TRS length, a commercial beam propagation method (BPM) based software has been used to simulate the coupling of the lasing (fundamental) mode from the SRS to the TRS. Fig. 4(a) shows the top view of the proposed structure in optimization. As previously described, once half of the light power in the lasing mode is coupled to the underneath slab waveguide in the TRS by the linearly reduced ridge width, we cut off the waveguide to form the front (output) facet. Since the half-coupling generates the most broadly expanded mode, the corresponding far-field will have smallest divergence angles. Apparently, the pulling down of the

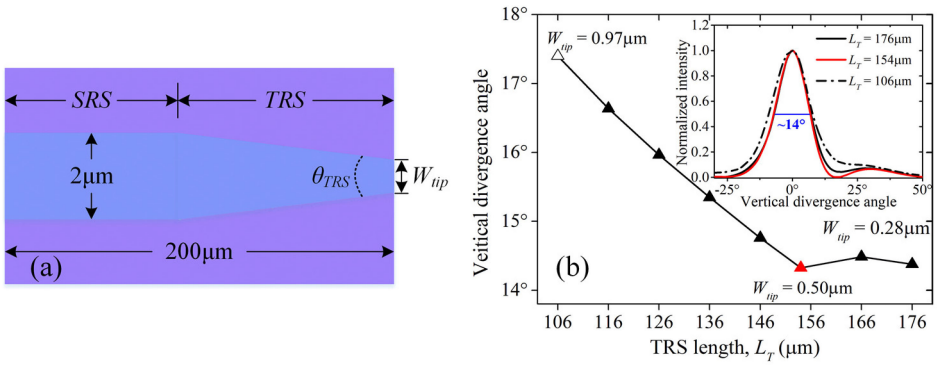

Fig. 4. (a) The top view of the proposed structure in optimization. (b) The vertical far-field divergence angle versus the TRS length with the transition angle fixed at 0.56°.

lasing mode power from the top ridge to the underneath slab waveguide can only happen at a TRS length beyond the propagation constant matching point. The TRS will have to be further extended after the matching point and the ridge width will then be narrower than 0.97 μm (at which the propagation constant of the top ridge waveguide becomes matched to the underneath slab waveguide). Knowing the constraint imposed to the total cavity length so as not to jeopardize the laser's dynamic performance, as well as the constraint to the SRS to TRS transition angle indicated by θ_{TRS} in Fig. 4(a) so as not to introduce any appreciable propagation loss, we managed to obtain an optimum solution by jointly tuning the TRS length and the transition angle, with 200 μm set as the fixed total cavity (TRS plus SRS) length and 1° as the upper limit of the transition angle. Actually, with a TRS length of 154 μm (SRS length of 46 μm) in a transition angle of 0.56°, half of the lasing mode power is coupled to the underneath slab waveguide and the vertical direction far-field divergence angle indeed reaches to its minimum value (about 14°) as shown in Fig. 4(b). The corresponding TRS ridge width at the front facet, denoted as W_{tip} in Fig. 4(a), is 0.5 μm, a value can still be handled by the standard photolithography and etching process without more complicated technique involved.

4. Device Performance

Through above design optimization, we have obtained a set of structural parameters that can effectively reduce the far-field divergence angles. We will then simulate the device performance by exploiting a direct numerical convolution model [28], [29]. Other than those FP laser parameters given in Table 1, we have had the rest device parameters summarized in Table 2. For comparison purpose, the result of a reference FP laser with the same parameters but in a straight ridge waveguide (i.e., with the full cavity as the SRS) is also shown.

Due to the shrinkage of the ridge width, the confinement factor decreases in the TRS. The modal gain will consequently decrease in the TRS, although the material gain doesn't change in the entire device. As the lasing mode is gradually pulled down, its evanescent tail actually has a smaller overlap with the heavily p-doped cladding layer where the internal loss appears due to the free-carrier absorption. As a result, the modal loss also decreases with the reduced ridge width in the TRS. We have calculated the variation of the confinement factor, the modal gain, and the modal loss along the TRS as shown in Fig. 5.

4.1 Static Characteristics

The calculated L-I curves of the proposed and the reference FP laser are shown in Fig. 6. The proposed FP laser almost has the same threshold current and a slightly increased slope efficiency

TABLE 2
Additional Laser Modeling Parameters

Parameter	Value	Unit
Reference laser ridge width	2	μm
Reference laser cavity length	200	μm
Ridge width in SRS	2	μm
SRS length	46	μm
Tip width in TRS	0.50	μm
TRS length	154	μm
Confinement factor in SRS	0.062	
Active region (well) total thickness	45	nm
Rear facet amplitude reflection coefficient	0.95	
Front facet amplitude reflection coefficient	0.32	
Group index	3.6	
Modal loss in SRS	12	cm^{-1}
Material gain coefficient	2700	cm^{-1}
Transparent carrier density	0.9×10^{18}	cm^{-3}
Characteristic temperature	60	K
Gain peak wavelength	1.31	μm
Linewidth enhancement factor	2	
Nonlinear gain saturation coefficient	7×10^{-17}	cm^{3}
SRH recombination coefficient	1.0×10^{9}	s^{-1}
Bimolecular non-radiative recombination coefficient	1.0×10^{-10}	$cm^{3}s^{-1}$
Auger recombination coefficient	3.5×10^{-29}	$cm^{6}s^{-1}$
Spontaneous emission coefficient	5×10^{-5}	

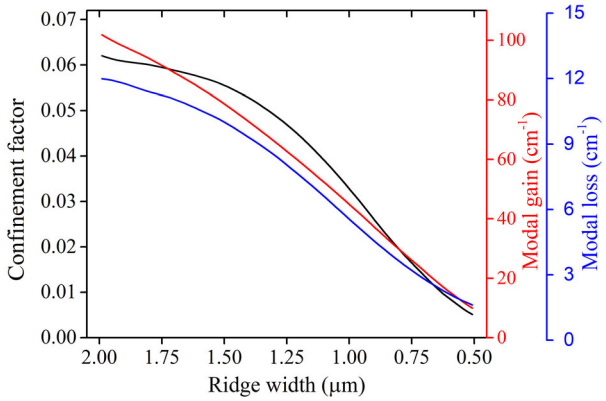

Fig. 5. Dependence of the confinement factor, the modal gain, and the modal loss on the ridge width in the TRS.

as compared to the reference one at both room (25 °C) and high (85 °C) temperatures. The surprising slope efficiency increase can be attributed to the drop of the modal loss in the TRS. It is worth mentioning that the radiation loss in the TRS is not considered in the simulation model, as it largely depends on the processing technique. We then need to keep in mind that the improvement on the slope efficiency may not be true in the fabricated real-world devices. However, it at least

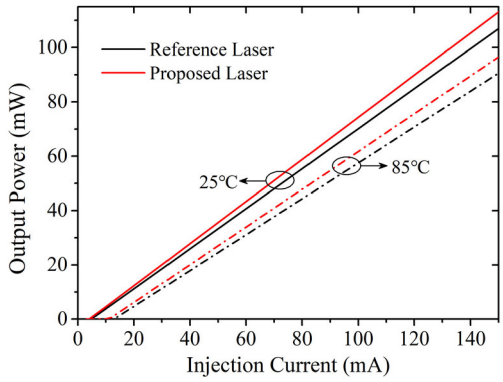

Fig. 6. Simulated L-I characteristics of the proposed and the reference FP laser.

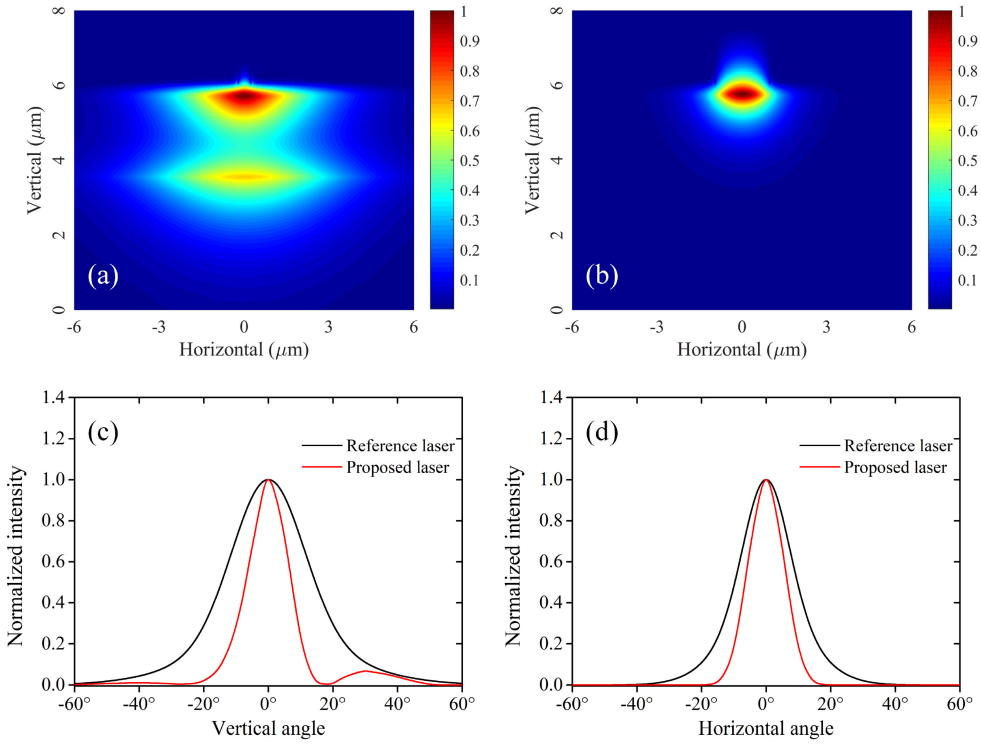

Fig. 7. Lasing (fundamental) mode profiles at the front (output) facet of (a) the proposed laser, and (b) the reference FP laser, respectively. Comparison between far-field divergence angles along (c) the vertical direction, and (d) the horizontal direction, respectively.

indicates that the proposed FP laser will unlikely have any appreciable degradation on its L-I characteristics.

The lasing (fundamental) mode profile at the front (output) facet of the proposed device is largely expanded compared to that of the reference FP laser, respectively shown in Figs. 7(a) and (b). Consequently, their divergence angles along the vertical and horizontal directions are significantly reduced, respectively shown in Figs. 7(c) and (d). For the proposed device, the divergence angles are now only 13.4°×14.3° (horizontal × vertical), as opposed to 19.8° × 28.5° in the reference FP laser. The small side lobe appeared in the far-field along the vertical direction in Fig. 7(c) is caused

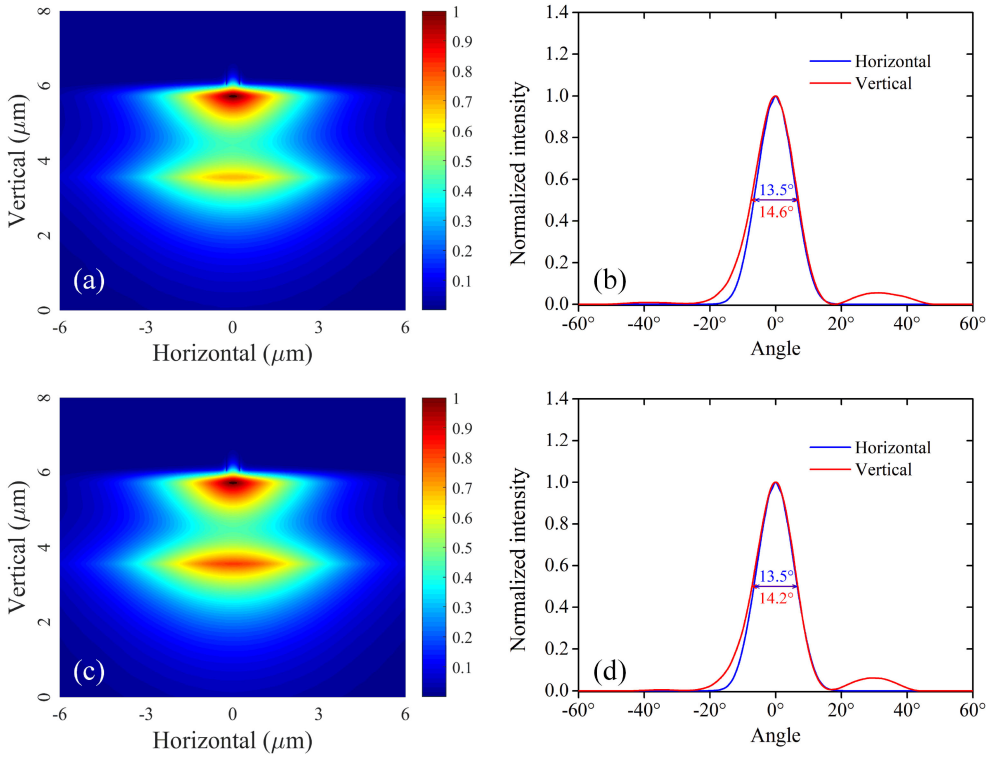

Fig. 8. The lasing mode profile (a) and the far-field divergence angles (b) under 105 °C for the active region and 85 °C for the rest structure, respectively. And the lasing mode profile (c) and the far-field divergence angles (d) under 85 °C for the entire structure. All the results are calculated at the front (output) facet of the proposed laser.

by the dual modal distribution [9]. The side lobe peak can be reduced by either raising the refractive index, or by reducing the thickness, of the spacer between the top ridge and the underneath slab waveguide. But it is not necessary in our case as the power taken by the side lobe is negligible.

The temperature impact on the far-field divergence angles is also studied. We find that under an ambient temperature of 85 °C, no appreciable changes can be found in the far-field divergence angles of the proposed laser, regardless of considering junction heating (so that the temperatures of the active region and the rest structure are set to 105 °C and 85 °C, respectively) or not (so that the temperature of the entire structure is set to 85 °C), as evidenced by Fig. 8, although the lasing mode profile does show minor changes.

4.2 Dynamic Characteristics

The calculated small-signal intensity modulation responses of the proposed and the reference FP laser are shown in Fig. 9. There is no significant deterioration on the modulation response of the proposed FP laser as compared to the reference one. The slight drawback on the proposed device AC performance is due likely to its reduced effective active region volume, which raises the carrier density and causes a differential gain reduction, as a phenomenological logarithmic material gain – carrier density dependence [30] has been used in our numerical model.

Figs. 10 and 11 exhibit the simulated eye-diagrams of the proposed and the reference FP laser under the data rates of 10 Gb/s and 25 Gb/s, respectively. No appreciable difference can be found in these diagrams and clear eye openings can be observed in all cases.

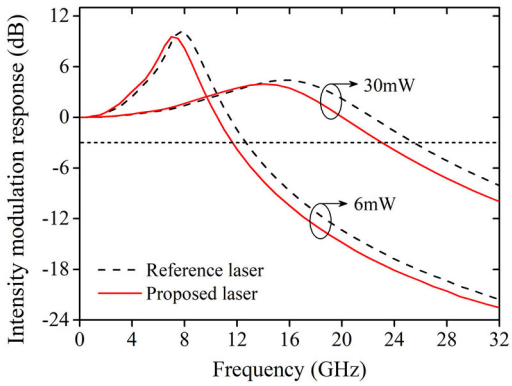

Fig. 9. Simulated small-signal intensity modulation responses of the proposed and the reference FP laser with different output powers.

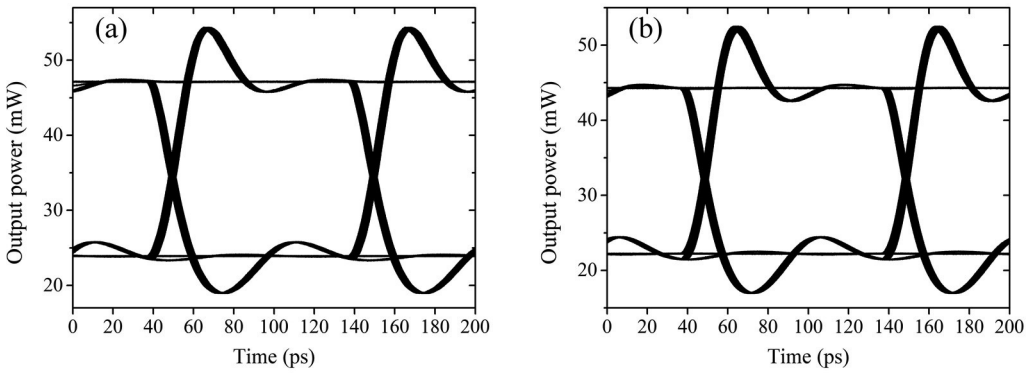

Fig. 10. Simulated 10 Gb/s eye-diagrams of (a) the proposed laser, and (b) the reference FP laser, respectively.

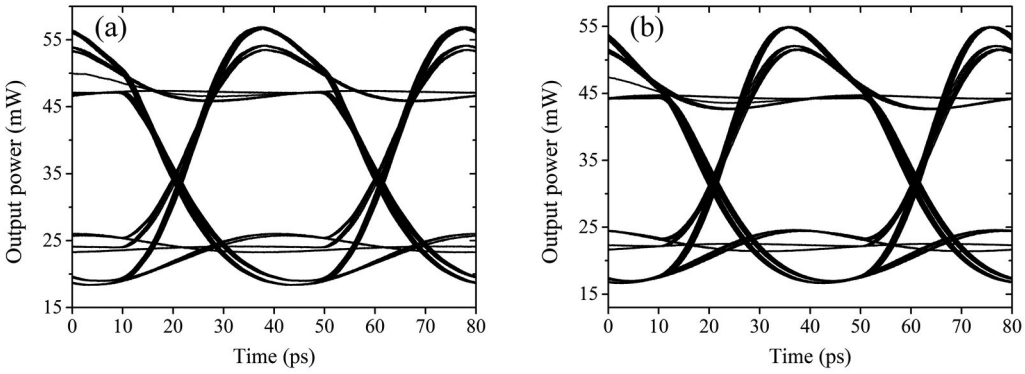

Fig. 11. Simulated 25 Gb/s eye-diagrams of (a) the proposed laser, and (b) the reference FP laser, respectively.

5. Conclusion

In conclusion, we have proposed a partially tapered ridge waveguide Fabry-Perot laser with a vertically coupled twin-waveguide structure. This regrowth-free device is fully compatible with the standard manufacturing technology of the conventional RW devices. The matching of the two waveguides in the tapered section only prevents the inserted underneath slab waveguide from

deteriorating the laser performance. The greatly expanded lasing mode profile at the front facet effectively reduces the laser far-field divergence angles, particularly the vertical divergence angle as otherwise it would be very difficult to cut it down by other means without regrowth involved. Numerical simulation result shows that the divergence angles of the proposed laser can be as low as 13° × 14° (horizontal × vertical), cut by about half in both directions as compared to the typical combination (20° × 29°) obtained from the reference RW FP laser. Simulated device static and dynamic performance also confirms that the proposed laser suffers no appreciable degradation as compared to the reference FP laser. All above features indicate that the proposed laser structure is an appealing improvement to conventional FP lasers for cost reduction in high-speed short-reach applications. Moreover, there is a potential to implement the same design idea to high-power pump lasers to avoid catastrophic optical damage at the output facet, as the largely expanded mode size surely dilutes the power intensity.

References

[1] M. Toda, "Two lens optical package and method of making same," US Patent 4,705,351 Patent Appl. 801,828, 1987.
[2] E. M. Kim and J. Peter, "Two Spherical Lens Optical Coupler," US Patent 4,842,391 Patent Appl. 152,958, 1989.
[3] C. G. Schriks, H. A. Van De Pas, J. W. Kokkelink, and H. F. J. J. Van Tongeren, "Optoelectronic device having a coupling comprising a lens and arranged between an optical transmission fiber and a semiconductor laser diode," US Patent 5,107,537 Patent Appl. 622,669, 1992.
[4] K. Shiraishi, N. Oyama, K. Matsumura, I. Ohishi, and S. Suga, "A fiber lens with a long working distance for integrated coupling between laser diodes and single-mode fibers," *J. Lightw.Technol.*, vol. 13, no. 8, pp. 1736–1744, Aug. 1995.
[5] I. Moerman, P. P. Van Daele, and P. M. Demeester, "A review on fabrication technologies for the monolithic integration of tapers with III–V semiconductor devices," *IEEE J. Sel. Topics Quantum Electron.*, vol. 3, no. 6, pp. 1308–1320, Dec. 1997.
[6] V. Vusirikala *et al.*, "GaAs-AlGaAs QW diluted waveguide laser with low-loss, alignment-tolerant coupling to a single-mode fiber," *IEEE Photon. Technol. Lett.*, vol. 8, no. 9, pp. 1130–1132, Sep. 1996.
[7] D. Vakhshoori *et al.*, "980nm spread index laser with strain compensated InGaAs/GaAsP/InGaP and 90% fibre coupling efficiency," *Electron. Lett.*, vol. 32, no. 11, pp. 1007–1008, 1996.
[8] G. Lin, S.-T. Yen, C.-P. Lee, and D.-C. Liu, "Extremely small vertical far-field angle of InGaAs-A1GaAs quantum-well lasers with specially esigned cladding structure," *IEEE Photon. Technol. Lett.*, vol. 8, no. 12, pp. 1588–1590, Dec. 1996.
[9] B. Qiu, S. D. McDougall, X. Liu, G. Bacchin, and J. H. Marsh, "Design and fabrication of low beam divergence and high kink-free power lasers," *IEEE J. Quantum Electron.*, vol. 41, no. 9, pp. 1124–1130, Sep. 2005.
[10] A. Pietrzak, P. Crump, H. Wenzel, G. Erbert, F. Bugge, and G. Trankle, "Combination of low-index quantum barrier and super large optical cavity designs for ultranarrow vertical far-fields from high-power broad-area lasers," *IEEE J. Sel. Topics Quantum Electron.*, vol. 17, no. 6, pp. 1715–1722, Nov. /Dec. 2011.
[11] M. Galarza *et al.*, "Mode-expanded 1.55-μm InP–InGaAsP Fabry–Pérot lasers using ARROW waveguides for efficient fiber coupling," *IEEE J. Sel. Topics Quantum Electron.*, vol. 8, no. 6, pp. 1389–1398, Dec. 2002.
[12] J. N. Walpole *et al.*, "Slab-coupled 1.3-μm semiconductor laser with single-spatial large-diameter mode," *IEEE Photon. Technol. Lett.*, vol. 14, no. 6, pp. 756–758, Jun. 2002.
[13] I. I. Novikov *et al.*, "High-power single mode ($>$1 W) continuous wave operation of longitudinal photonic band crystal lasers with a narrow vertical beam divergence," *Appl. Phys. Lett.*, vol. 92, no. 10, 2008, Art. no. 103515.
[14] L. Liu *et al.*, "Design and analysis of laser diodes based on the longitudinal photonic band crystal concept for high power and narrow vertical divergence," *IEEE J. Sel. Topics Quantum Electron.*, vol. 21, no. 1, pp. 440–446, Jan. /Feb. 2015.
[15] J. P. Donnelly *et al.*, "AlGaAs–InGaAs slab-coupled optical waveguide lasers," *IEEE J. Quantum Electron.*, vol. 39, no. 2, pp. 289–298, Feb. 2003.
[16] C. Stagarescu, A. A. Behfar, and N. S.-k. Kwong, "Lasers with beam-shape modification," US Patent 9,865,993 B2 Patent Appl. 15/160,895, 2018.
[17] Masahiro Kito *et al.*, "High slope efficiency and low noise characteristics in tapered-active-stripe DFB lasers with narrow beam divergence," *IEEE J. Quantum Electron.*, vol. 35, no. 12, pp. 1765–1770, Dec. 1999.
[18] P. Doussiere *et al.*, "Tapered active stripe for 1.5-μm InGaAsP/InP strained multiple quantum well lasers with reduced beam divergence," *Appl. Phys. Lett.*, vol. 64, no. 5, pp. 539–541, 1994.
[19] K. Takemasa, M. Kubota, and H. Wada, "1.3-μm AlGaInAs-InP buried-heterostructure lasers with mode profile converter," *IEEE Photon. Technol. Lett.*, vol. 12, no. 5, pp. 471–473, May 2000.
[20] V. Vusirikala *et al.*, "High butt-coupling efficiency to single-mode fibers using a 1.55-μm InGaAsP laser integrated with a tapered ridge mode transformer," *IEEE Photon. Technol. Lett.*, vol. 9, no. 11, pp. 1472–1474, Nov. 1997.
[21] X. Sun, H.-C. Liu, and A. Yariv, "Adiabaticity criterion and the shortest adiabatic mode transformer in a coupled-waveguide system," *Opt. Lett.*, vol. 34, no. 3, pp. 280–282, 2009.
[22] G. Roelkens, D. Van Thourhout, R. Baets, R. Nötzel, and M. Smit, "Laser emission and photodetection in an InP/InGaAsP layer integrated on and coupled to a Silicon-on-Insulator waveguide circuit," *Opt. Express*, vol. 14, no. 18, pp. 8154–8159, Sep. 2006.
[23] A. Yariv and X. Sun, "Supermode Si/III-V hybrid lasers, optical amplifiers and modulators: A proposal and analysis," *Opt. Express*, vol. 15, no. 15, pp. 9147–9151, Jul. 2007.

[24] G. Allen Vawter, C. T. Sullivan, J. R. Wendt, R. E. Smith, H. Q. Hou, and J. F. Klem, "Tapered rib adiabatic following fiber couplers in etched GaAs materials for monolithic spot-size transformation," *IEEE J. Sel. Topics Quantum Electron.*, vol. 3, no. 6, pp. 1361–1371, Dec. 1997.
[25] V. M. Menon, F. Xia, and S. R. Forrest, "Photonic integration using asymmetric twin-waveguide (ATG) technology: Part II—devices," *IEEE J. Sel. Topics Quantum Electron.*, vol. 11, no. 1, pp. 30–42, Feb. 2005.
[26] A. W. Fang, E. Lively, Y.-H. Kuo, D. Liang, and J. E. Bowers, "A distributed feedback silicon evanescent laser," *Opt. Express*, vol. 16, no. 7, pp. 4413–4419, Mar. 2008.
[27] M. Lamponi *et al.*, "Low-Threshold heterogeneously integrated InP/SOI lasers with a double adiabatic taper coupler," *IEEE Photon. Technol. Lett.*, vol. 24, no. 1, pp. 76–78, Jan. 2012.
[28] X. Li, *Optoelectronic Devices: Design, Modeling, and Simulation.* Cambridge, England: Cambridge Univ. Press, 2009.
[29] J. Fu, Y. Xi, X. Li, and W.-P. Huang, "Narrow spectral width FP lasers for high-speed short-reach applications," *J. Lightw. Technol.*, vol. 34, no. 21, pp. 4898–4906, Nov. 2016.
[30] T. Suhara, *Semiconductor Laser Fundamentals*. New York: Marcel Dekker, Inc., 2004.